Investigation of Corrosion Assisted Crack Growth in an Intermediate Size Pressure Vessel at Elevated Water Temperatures

Kussmaul, K., D. Blind, R. Gillot, and W. Burr, MPA Stuttgart

3rd International Conference on Biaxial / Multiaxial Fatigue, April 3 - 6, 1989, Stuttgart, FRG

Abstract

Within the framework of the research program "Integrity of Components (FKS)" an intermediate size welded pressure vessel (ZB 1) was loaded with hot water at 60°C and 288°C by internal pressure cycles and hydrotests to initiate and grow artificial and natural cracks. The water chemistry, especially with regard to the oxygen content and conductivity, turned out to be at worst case conditions. Total crack growth after 28.348 cycles, interrupted by several hydrotests at 60°C, ranged between a few millimeters and 57,2 millimeters, depending on the size and location of the original crack.

After completion of the cyclic pressure tests the cracked areas were removed from the vessel for metallografical and fractografical examinations. By these results a correlation between the crack depths at the various load cycles, the numerical predictions, and the nondestructive examinations during the tests was possible. It turned out that the biaxial state of stress has no influence on the crack growth rate for longitudinal and circumferential cracks.

The work on which this report is based was sponsored by the Federal Minister for Research and Technology (BMFT), the industry consortium Integrity of Components, and the United States Nuclear Regulatory Commission (USNRC). The responsibility for the content, however, only have the authors.

1. Introduction

One task of the research program "Integrity of Components (FKS)" /1/ concentrated on static and cyclic internal pressure tests at 60°C and 288°C. An underground test facility of the Großkraftwerk Mannheim AG (GKM) power plant was used for the ZB 1 pressure vessel tests. Several patches containing prefatigued notches on the inner and outer surface as well as natural cracks in the base material were inserted into the cylindrical vessel wall by longitudinal and circumferential welds. No post-weld heat treatment was applied for one of the three patches. The general objectives of the tests were

- to load the vessel by hydrotests and under operational conditions in order to produce crack propagation in the range of several centimeters

- to locate the cracks and to monitor crack growth by an acoustic emission analysis

- to measure crack growth by means of nondestructive testing, such as ultrasonics, potential drop method, magnetic particle testing, etc.

- to verify the actual crack length for each step of the test and to compare these values with the measured and precalculated ones

- to investigate the influence of hot water corrosion due to a highly oxygenated water.

After completion of the internal pressure tests the cracked patches and welds were removed from the vessel by torch-cutting and by trepanning. By the results of the final nondestructive as well as metallografical and fractografical examinations of selected areas a correlation between the crack depths at the various load cycles and the precalculations, the nondestructive examinations, and the acoustic emission analysis was possible.

2. Test Vessel ZB 1

The overall dimensions of the intermediate size test vessel and the prefatigued notches are shown in Fig. 1. The material of the rectangular patch S1 containing the three notches was machined from a plate of A 533 B Cl.1 /2/, the other patch S3 was made of the material 20 MnMoNi 5 5 (similar to A 533 B Cl.1). The wall thickness of 120 mm was about 15% smaller than the one of a pressure vessel of a boiling water reactor (BWR). When the test was started, the relative depth of the three flaws A, B, and C ranged from a/W = 0,25 to 0,47.

The test vessel was loaded by 8 hydrotests and 21.000 load cycles at 60°C, and by 7.340 more load cycles at 288°C /3/. The load spectrum is shown in Fig. 2. The internal pressure of 240 bar caused a hoop stress in the cylindrical vessel wall of 160 N/mm^2, which corresponds to the hoop stress in a BWR vessel at operating conditions. The time needed for each load cycle was between 0,5 min at 60°C and 3 min at 288°C. The load steps A, B, and 1 through 7 (A, 1, 4, and 7 are hydrotests) were conducted in a period of 6 weeks, it took 26 more weeks to complete the tests at 288°C.

The test loop was filled with water from the condenser loop of the GKM power plant. The water chemistry deteriorated during the test runs because of the lack of a demineralizing system and the contact of the water with air in a feedwater tank. This caused an increase in the oxygen content up to the saturation level of 8 ppm.

3. Crack Propagation

The purpose of the cyclic internal pressure loading was to produce crack propagation in the order of several centimeters. This was realized by loading prefatigued notches and longitudinal and circumferential welds with natural cracks.

3.1 Crack Propagation in the Prefatigued Notches

According to the table in Fig. 1 the total crack propagation was 48,8 mm for flaw A, 57,2 mm for flaw B, and 4,2 mm for flaw C. The flaws A and B were located on the inner surface, flaw C on the outer surface of the vessel. As an example for the others, flaw B will be presented in detail in this paper.

Fig. 3 shows flaw B at the end of the test after 28.348 load cycles /4/. The flaw grew approximately 65 mm on each side in longitudinal direction. Several secondary cracks parallel to the main crack path can be seen in the second half of the crack propagation, this corresponds to the test temperature of 288°C. In addition, the effect of corrosion is evident by the large number of cavities on the inner surface of the vessel.

After the test, flaw B was saw-cut into several sections and opened, Fig. 4. Starting from the center of the flaw the first two semi-elliptical crack fronts are the tip of the machined and prefatigued notch, resp. The adjacent bright portion of the fracture surface is the result of the cyclic loading at 60°C, the loading at 288°C caused the crack growth demonstrated by the outer, dark grey section.

Section A of Fig. 4 is shown in datail in Fig. 5. The different load steps according to Fig. 2 are separated by clearly defined lines which were caused by stable crack growth during the hydrotests. With these marked crack fronts a reliable correlation between the different load steps and the crack propagation is possible.

According to Fig. 3, the crack propagation in longitudinal direction occured on a straight path. This is also true for the propagation in the radial direction, Fig. 6. Especially at the location of hydrotests there is a tendency for small secondary cracks, which in most cases branched off the main crack path in an angle of 20 to 30° and in no case exceeded a length of 0,4 mm. It is of special interest that the branching started symme-

trically to both sides of the main crack, and that in most cases one, in some cases both cracks turned back to the centerline after a few tenths of a millimeter. At the fracture surface corresponding to a test temperature of 60°C no secondary cracks were found in any of the three flaws. The general direction of the main crack path is not influenced by these cracks.

Fig. 7 shows a close-up view of the fracture surface at the end of load step 9 (288°C), the two hydrotests 10 (60°C), and the first cycles of step 11 (288°C). One clearly can see fatigue striations caused by the cyclic loading during steps 9 and 11. The two hydrotests, separated by ten load cycles, can be identified by a stable crack growth of 0,06 and 0,07 mm, resp. The secondary cracks on the fracture surface correspond to section C of Fig. 6.

Crack branching in a more pronounced form was found in the cylindrical wall of the pressure vessel of the decommissioned HDR plant /5/ (superheated steam reactor near Frankfurt/Main), Fig. 8. This investigation was part of the THEZ-series (thermal shock of the cylindrical vessel wall) of the HDR Safety Program /6/, where loading by cyclic thermal shock was applied. The circumferential crack started from a 9 mm deep blunt notch and was grown by 6500 load cycles in three test blocks. During the two stops in between the vessel was statically loaded at different pressure levels and temperatures for 100 h and 140 h, resp. In this case, the high temperature water also had an elevated oxygen content.

3.2 Crack Propagation in Welds

At the beginning of the test series a second rectangular patch of the degraded material KS07C (patch S2, dimensions 1500 x 700 mm^2, Fig. 2) with hydrogen induced multiple cracks was welded into the cylindrical vessel wall. After a hydrotest and 5.000 load cycles (Fig. 2, steps A and B) it was replaced on site by the patch S3, machined from a plate of 20 MnMoNi 5 5 reactor grade material.

The welds were inspected by the dye penetrant method, defects in the weld roots were repaired. A final stress relief heat treatment was not applied.

After 23.340 load cycles at 60°C and 288°C and 7 hydrotests at 60°C (Fig. 2, step 1 through 12) the patch S3 was removed from the vessel by torch-cutting. The inner surface after a final nondestructive examination (NDE) is shown in Fig. 9. The bright rectangle from the magnetic particle testing marks the location of the longitudinal and circumferential welds. Three trepans (B1 through B3, diameter 100 mm) were taken from the welds at locations where the deepest cracks were expected.

Two sections of the cracked root of the longitudinal weld LN 1 are shown in Fig. 10. In both cases, numerous cracks on either side of the root can be seen. While the preferential orientation is in the longitudinal direction, there are some cracks with a circumferential orientation. The bottom picture of Fig. 10 depicts an area of a repair weld with cracks at the transition from the weld to the base material.

In order to further investigate the morphology of the fracture surface, the cracks of the three trepans were opened. Comparable to the appearance in the three flaws, the various load steps can be correlated to clearly visible stripes on the fracture surface, Fig. 11. The different lines in Fig. 11b correspond to crack growth caused by cyclic loading on one test day, Fig. 11c, or to hydrotests, Fig. 11d. Due to an extremely corroded fracture surface no statements can be made for the load steps 1 through 8 with a total crack propagation of 8,9 mm.

Fig. 12 shows a close-up view of one of the stripes of step 9 (Fig. 11b). This section of the fracture surface corresponds to a total crack growth of 0,186 mm, caused by 204 load cycles between 150 and 250 bar at 288°C. This test sequence was conducted after a stop of 18 days with temperatures between 10°C and 288°C.

The crack growth rate da/dN at the beginning of the cyclic

loading is more than twice as high as in the second half of the day. The plateau reached after 80 load cycles is slightly above the value derived from the K_I-calculation and the da/dN-curve for water according to ASME, Sect. XI /7, 8/. Tests to determine the da/dN-values for the particular vessel conditions (vessel material, water chemistry) were not conducted. After an overnight stop of 8 hours at 150 bar and 288°C, da/dN is high again during the first cycles of the following day, see right end portion of Fig. 12.

Similar investigations were conducted on cracks in the two circumferential welds of the patch. A close-up view of a fracture surface of section 4 of Fig. 9 is shown in Fig. 13. Compared to the longitudinal crack shown in Fig. 11, the fracture surface of the circumferential ones is extremely rough without clearly visible lines separating the different test days.

After removing the corrosion layers from the fracture surface, striations only could be found at the crack tip, Fig. 14. They were caused by load cycles of the last test days of step 11, ranging between 100 and 250 bar at 288°C. Calculations for finite length circumferential part-through cracks in vessels /9/ assuming an average crack depth of 20 mm and a total crack length of 700 mm (according to the width of the patch) yield a stress intensity factor of $\Delta K = 13\ \text{MPa}\ m^{1/2}$. According to /8/ this corresponds to a crack growth rate of $2{,}5.10^{-4}$ mm/load cycle which is one fourth of the measured value at test begin.

With an increasing number of load cycles, da/dN in Fig. 14 decreases to lower values. This behaviour is similar to the one described in Fig. 12. Due to the rough fracture surface of the circumferential cracks a more detailed evaluation can not be made. It seems to be evident, however, that the overall crack behaviour of longitudinal and circumferential cracks is similar.

An explanation for that behaviour can be the corrosion of the oxygen saturated water at the crack tip during the stops. Thereby hydrogen embrittlement in the region of the crack tip may

occur /10 through 13/. Consequently a decrease in toughness would result which leads to an increase of the da/dN-value. After a number of load cycles the crack passes the embrittled zone and propagates into the base metal with undegraded toughness. Other explanations were presented in /14/.

Similar crack growth behaviour in high temperature water was found during fracture mechanics tests under static load /15/ as well as in corrosion fatigue experiments /16, 17/. These cases, however, are different with regard to loading and water conditions.

4. Numerical Determination of the Crack Propagation

Before starting the test, the expected crack growth of the flaws A, B, and C was precalculated for the different load steps. Numerical solutions for the different stress intensity factors of semi-elliptical surface cracks are available /7/, the crack growth rates da/dN were taken from /8/ for water (flaws A and B) or air (flaw C), resp.

According to ASME, the da/dN-curves are upper bound (conservative) values. Therefore, it should be expected that the actual crack depth is always below the predicted one. This could be shown by the fractografical results for the tests conducted at 60°C (load steps A, B, and 1 through 7). During that test period the precalculation always overestimated the actual crack depth.

Major differences were noticed when the test temperature was increased to operational conditions (288°C, load steps 8, 9, and 11). In this case the two flaws on the inner surface of the vessel wall grew faster than predicted. The crack depth of flaw C on the outer vessel wall always stayed behind the calculated value.

For further clarification, the calculated and measured crack propagation of flaw B with the highest crack growth rate is com-

piled in Table 1. One can see that at the end of the tests at 60°C (step 6) the calculated crack depth is 19% longer than the measured one according to Fig. 5. For the load steps B through 5 a reliable correlation between crack length and load cycles is not possible due to corrosion effects on the fracture surface.

At the tests at 288°C (load steps 8, 9, and 11), the overestimation continually decreases, till finally the calculated crack depth falls behind the measured values. This discrepancy turned from 15% overestimation at the end of step 8 to a slight underestimation at the end of step 11.

It seems to be evident that the reason for that behaviour is corrosion again. Like in trepan B2 of patch S3, a higher crack growth rate after overnight or repair stops in the first 100 cycles well above the da/dN-values of ASME, Sect. XI caused an increase of the crack growth.

5. Summary

An intermediate size test vessel with prefatigued notches and natural cracks was loaded by 28.348 internal pressure cycles at 60°C and 288°C. The whole test series lasted 12 months.

After the tests the crack faces were opened and further investigated. The metallografic and fractografic examinations can be summarized as follows:

- The crack growth of the prefatigued notches ranged from 4,2 mm (flaw C on outer surface, no corrosion) to 48,8 mm (flaw A on inner surface) and 57,2 mm (flaw B on inner surface).

- The natural cracks in the welds of patch S3 grew to a maximum depth of approximately 50 mm.

- For the test series conducted at 288°C a reliable correlation between the crack length and the particular load steps was possible. Due to corrosion effects, this correlation could not be made for the tests at 60°C.

- In the three prefatigued notches, the macroscopic crack propagation was on a very straight path. At 60°C no secondary cracks could be found on the fracture surface. At operating conditions (288°C) numerous secondary cracks branched off the main crack in an angle of 20 to 30°, especially at the locations of the hydrotests. These secondary cracks stopped at a depth of less than 0,4 mm.

- During stops at the 288°C-tests, especially those over night, a minimum pressure of 100 bar (to prevent evaporation of the water) and the temperature were held constant. The fractografical examination of the natural longitudinal and circumferential cracks in the welds of patch S3 showed a clear increase in the crack growth rate da/dN after stops.

- After a number of cycles (in the order of 100) da/dN decreased to a lower value corresponding to the ASME-curves and then stayed constant. This behaviour is believed to be caused by corrosion embrittlement at the crack tip during the stops due to the oxygen saturated water of the test loop.

- A correlation between the crack depths at the various load cycles, the numerical predictions, and the nondestructive examinations during the test was possible. Insofar, the applied analytical tools could be validated. It turned out that the biaxial state of stress has no influence on the crack growth rate for longitudinal and circumferential cracks.

References

/1/ Kussmaul, K., J. Föhl, and E. Roos:
Some Conclusions With Regard to the Safety Assessment of Cracked Components Drawn From the Research Program "Integrity of Components (FKS II)" at the Present State.
Nuclear Engineering and Design, Vol. 102, No.3, pp. 397-418, North-Holland Physics Publishing Division, Amsterdam, 1987

/2/ Hutton, P.H., R.J. Kurtz, and R.A. Pappas:
Acoustic Emission Monitoring of ZB 1 Intermediate Scale Vessel Test.
9. MPA-Seminar, Stuttgart, October 13 and 14, 1983,
Nuclear Engineering and Design, Vol. 84, No. 2, pp. 171-178, North-Holland Physics Publishing Division, Amsterdam, 1985

/3/ Gillot, R. and H. Beyer:
Innendruckversuche am Zwischenbehälter ZB 1 (KS 20).
Research Program "Integrity of Components", TWB 12/2, 1984

/4/ Burr, W., U. Coehne, U. Eisele, and R. Gillot:
Nachuntersuchungen am Zwischenbehälter ZB 1 (KS 20)
- Metallkunde, ZfP, Großproben -.
Research Program "Integrity of Components", TWB 12/3, 1987

/5/ Stegmeyer, R., E. Roos, and H. Diem:
Crack Initiation and Crack Propagation at the Cylinder Wall of the HDR Pressure Vessel Under Cyclic and Pressurized Thermal Shock Loading.
Third Int. Conference on Biaxial/Multiaxial Fatigue, Stuttgart, April 3 through 6, 1989

/6/ HDR Safety Program, Phase II: PHDR-Report No. 05.19/84.
Kernforschungszentrum Karlsruhe, January 1984

/7/ ASME Boiler and Pressure Vessel Code, Section XI, Article A-3000: Method for Determining Stress Intensity Factor, 1986

/8/ ASME Boiler and Pressure Vessel Code, Section XI, Article A-4000: Material Properties, 1986

/9/ Zahoor, A.:
Closed Form Expressions for Fracture Mechanics Analysis of Cracked Pipes.
Journal of Pressure Vessel Technology, Vol. 107, pp. 203-205, May 1985

/10/ Törrönen, K., H. Hänninen, H. Cullen, and W.H. Cullen:
Mechanisms of Environment Assisted Cyclic Crack Growth of Nuclear Reactor Pressure Vessel Steels.
Proceedings IAEA Specialists' Meeting on Subcritical Crack Growth, Freiburg, FRG, May 13-15, 1981, NUREG/CP-0044, Vol. 2, pp. 27-66, 1983

/11/ Hänninen, H. and I. Aho-Mantila:
Umgebungsinduzierte Rißbildung bei Werkstoffen in druckführenden Bauteilen von Leichtwasserreaktoren.
Der Maschinenschaden 59, Heft 4, pp. 154-165, 1986

/12/ Ford, F.P.:
Status of Research on Environmentally Assisted Cracking in LWR Pressure Vessel Steels.
The 1987 Pressure Vessel and Piping Conference, San Diego, California, June 28 - July 2, 1987, PVP Vol. 119, 1987

/13/ Magdowski, R.M. and M.O. Speidel:
Die Spannungsrißkorrosion von niedrig legierten Vergütungsstählen in Wasser.
Ergebnisse der Werkstoff-Forschung, Band 2: Spannungsrißkorrosion von Stahl in Wasser, Verlag Thubal-Kain, pp. 117-142, 1988

/14/ Tenckhoff, E., M. Erve, E. Lenz, and G. Vazoukis:
Environmentally Assisted Crack Growth in Low Alloy Steels - Results and Their Relevance to LWR-Components -

14. MPA-Seminar, Stuttgart, FRG, October 6 and 7, 1988,
to be published in Nuclear Engineering and Design

/15/ Kussmaul, K. and B. Iskluth:
Environmentally Assisted Crack Growth in a Low Alloy Boiler Steel in High Temperature Water Containing Oxygen.
14. MPA-Seminar, Stuttgart, October 6 and 7, 1988,
to be published in Nuclear Engineering and Design

/16/ Blind, D., D. Sturm, and H. Trunk:
Electron Micrografical Investigations of Corrosion Fatigue Surface Developed Under Pressure Water Reactor Conditions.
Proceedings IAEA Specialists' Meeting on Subcritical Crack Growth, Freiburg, FRG, May 13-15, 1981, NUREG/CP-0044,
Vol. 2, pp. 67-90, 1983

/17/ Van der Sluys, W.A. and R.H. Emanuelson:
Fatigue Crack Growth in Reactor Pressure Vessel Materials and Light Water Reactor Environments.
14. MPA-Seminar, Stuttgart, FRG, October 6 and 7, 1988,
to be published in Nuclear Engineering and Design

load step	temp. °C	$\Delta\sigma_{hoop}$ [1] MPa	ΔK_I [2] MPa $\sqrt{m}$	da/dN [3] 10^{-3} mm/cycle	cycles	Δa/mm	a_{total}/mm calculated	a_{total}/mm measured [4]	$\frac{a_{calc.}}{a_{meas.}}$
B	60	90	23	1,0	5000	5,0	46,2	-	-
2	60	144	39	2,5	2000	5,0	51,2	-	-
3	60	64	18	1,3	6000	7,8	59,0	-	-
5	60	144	44	3,3	2000	6,6	65,6	-	-
6	60	64	21	1,8	6000	10,8	76,4	64,4	1,19
8	288	100	35	3,3	2000	6,6	83,0	71,9	1,15
9	288	66	24	2,5	4000	10,0	93,0	88,4	1,05
11	288	100	38	3,5	1342	4,7	97,7	98,4	0,99

[1] from Fig. 2
[2] ASME, Section XI, Article A-3000 /5/
[3] ASME, Section XI, Article A-4000 /6/
[4] see Fig. 5

Table 1: Comparison of calculated and measured crack growth, longitudinal flaw B on inner surface

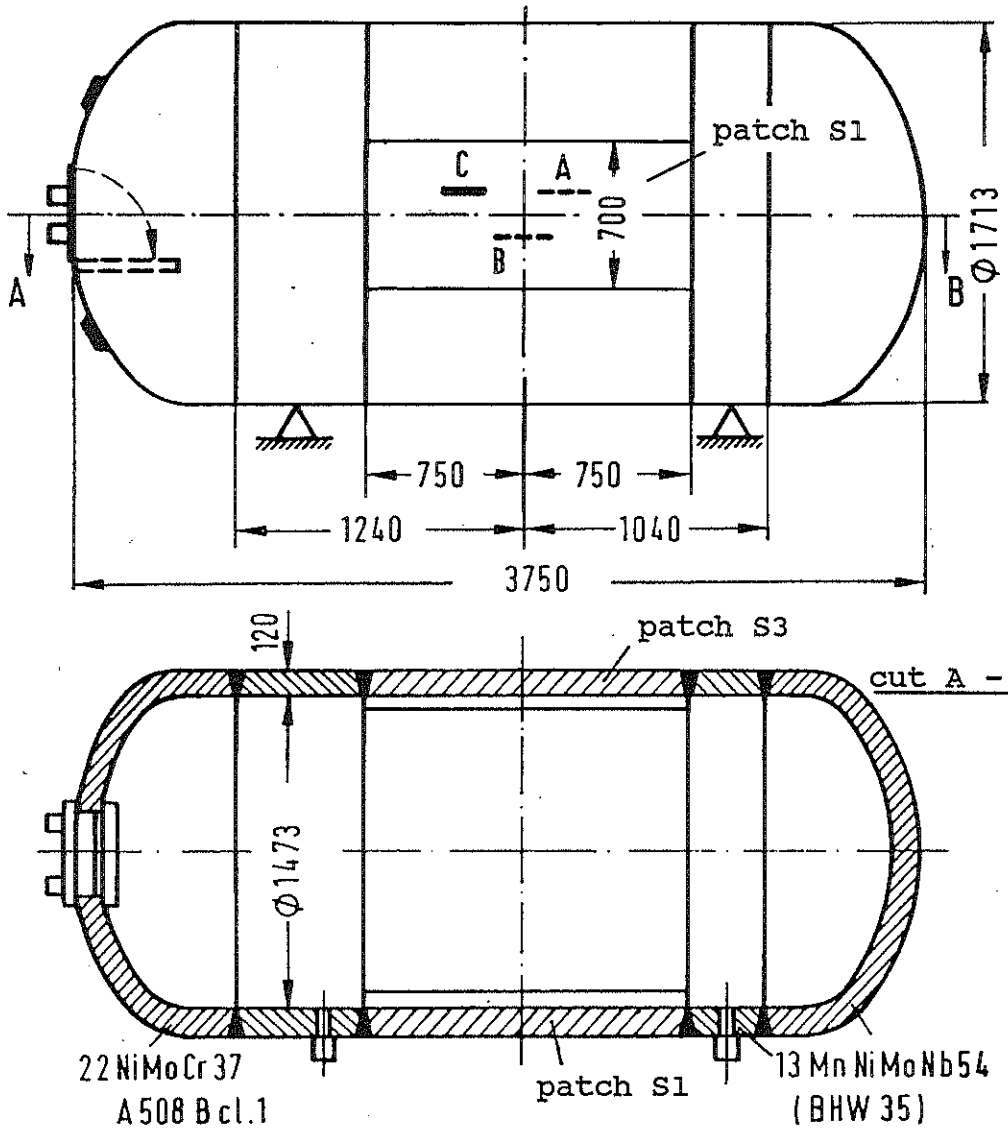

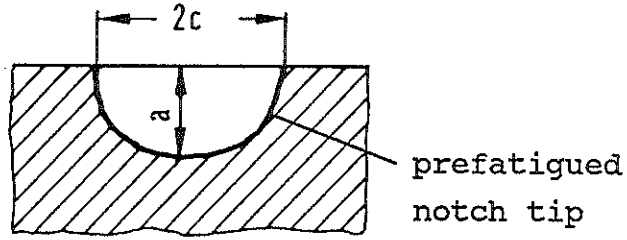

flaw	begin of test			end of test			
	2c/mm	a/mm	a/W	2c/mm	a/mm	a/W	Δa/mm
A	61,0	30,0	0,25	151,0	78,8	0,66	48,8
B	84,0	41,2	0,34	212,0	98,4	0,82	57,2
C	190,0	55,8	0,47	190,0	60,0	0,50	4,2

Fig. 1: Intermediate size pressure vessel ZB 1, dimensions of the vessel and the longitudinal flaws A, B, and C

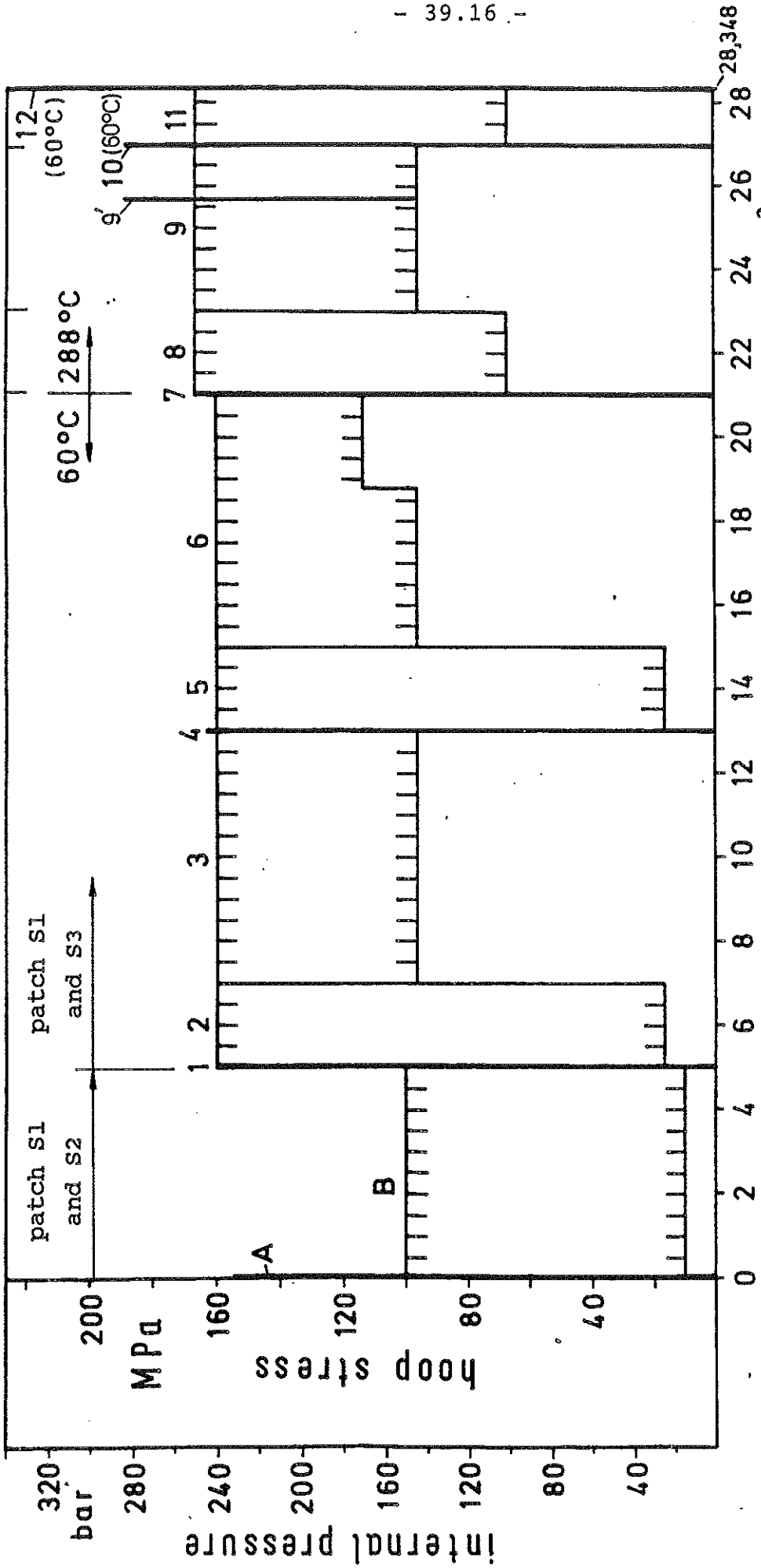

Fig. 2: Load spectrum of the ZB 1 pressure vessel tests, hydrotests A, 1, 4, 7, 10, and 12 at 60°C, hydrotest 9' at 288°C

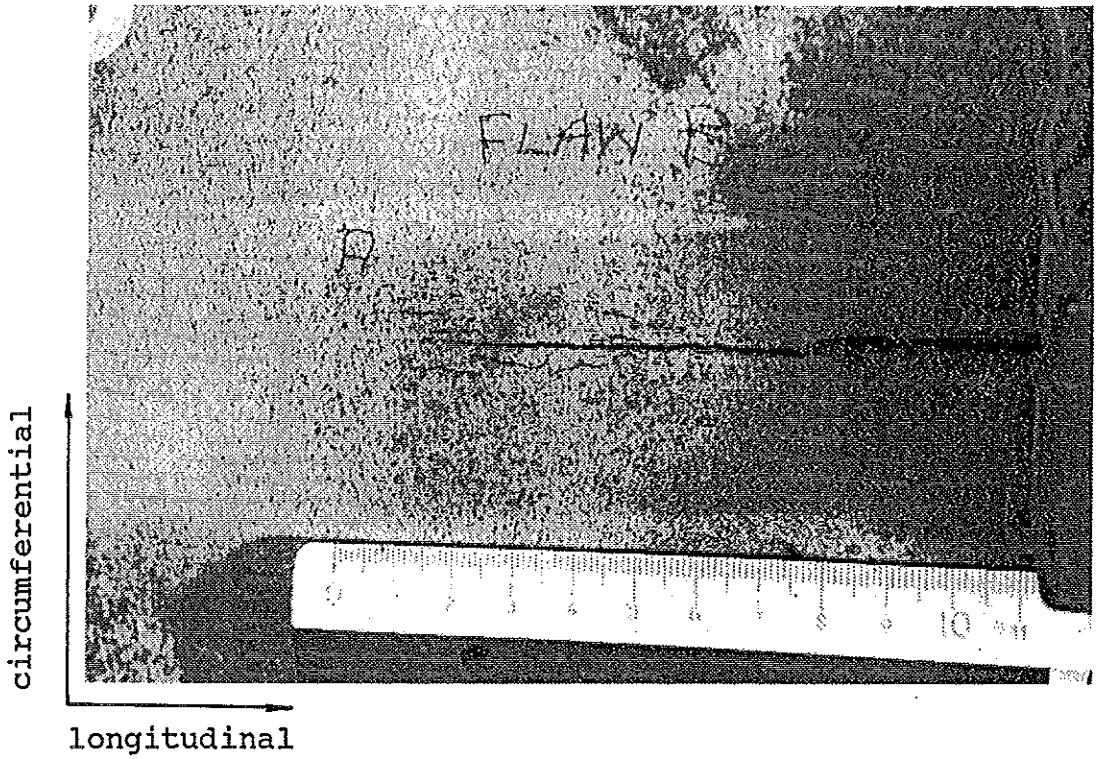

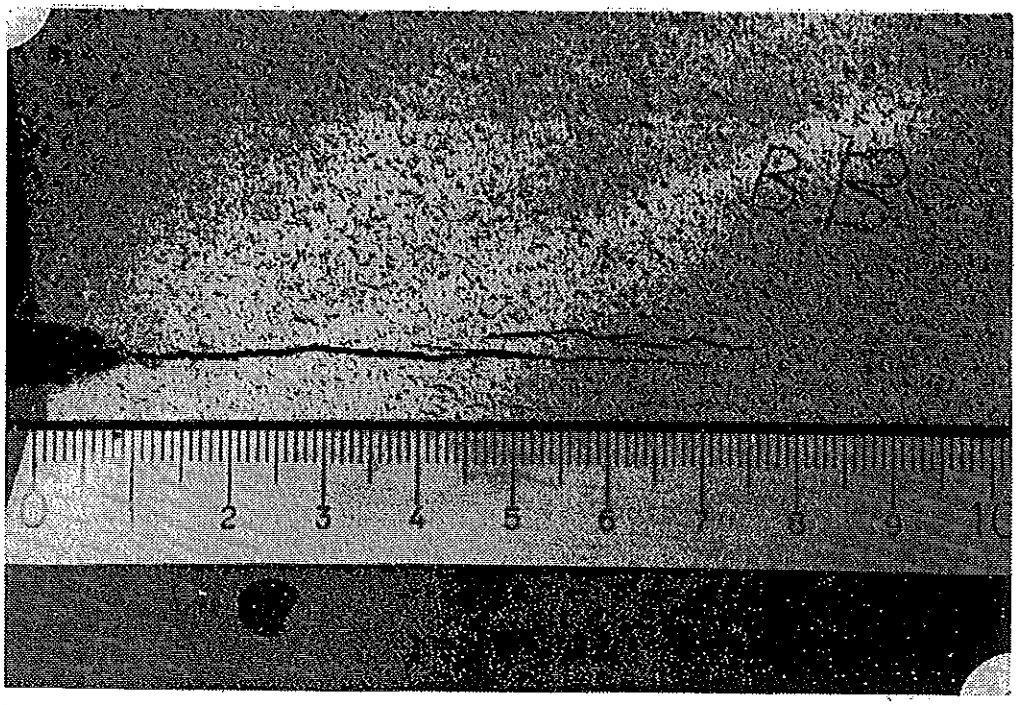

Fig. 3: Crack growth of longitudinal flaw B after 28.348 load cycles (end of test)
top: left side of flaw B, bottom: right side of flaw B

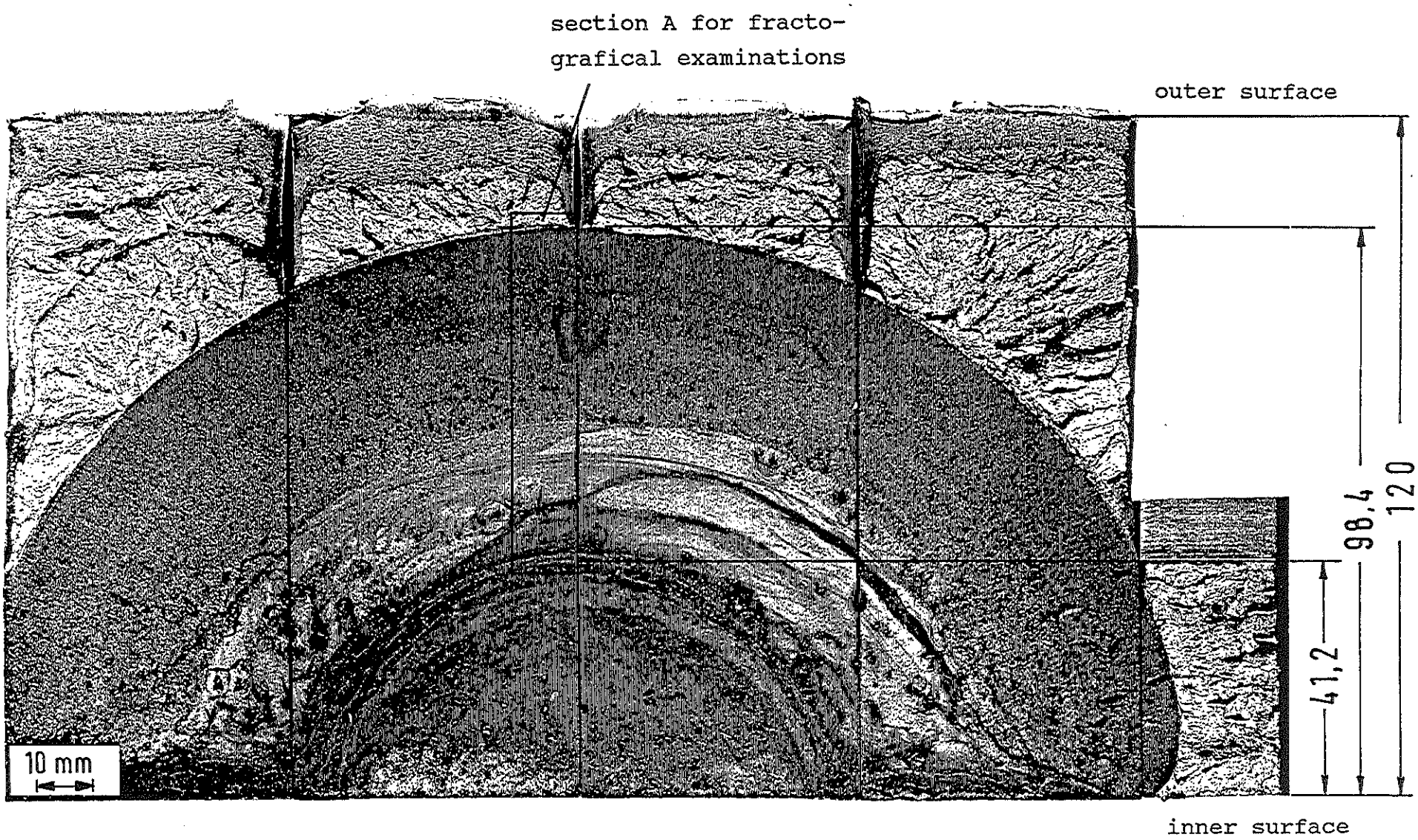

Fig. 4: Fracture surface of longitudinal flaw B after 28.348 load cycles (end of test)

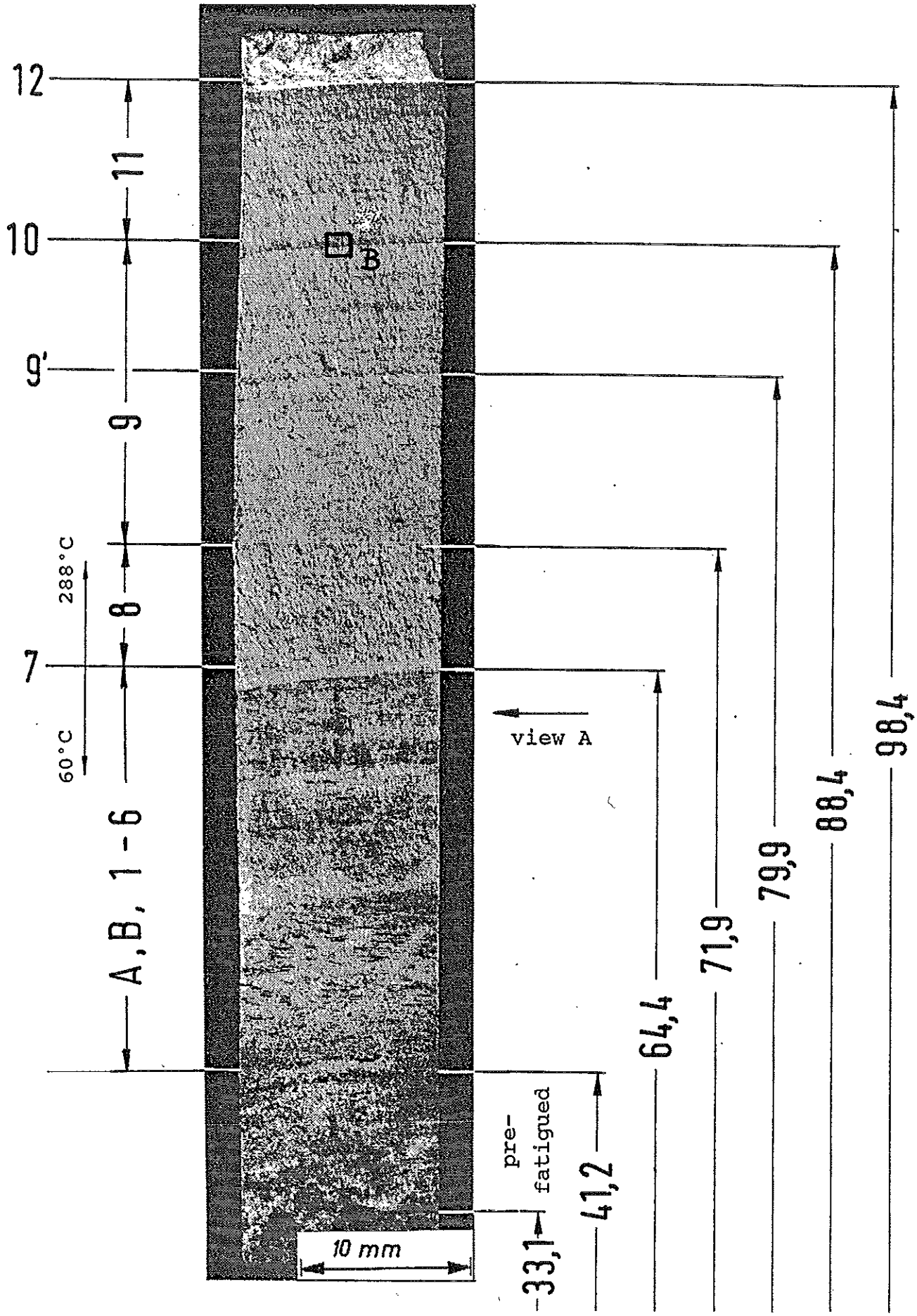

Fig. 5: Section A of Fig. 4, total crack propagation

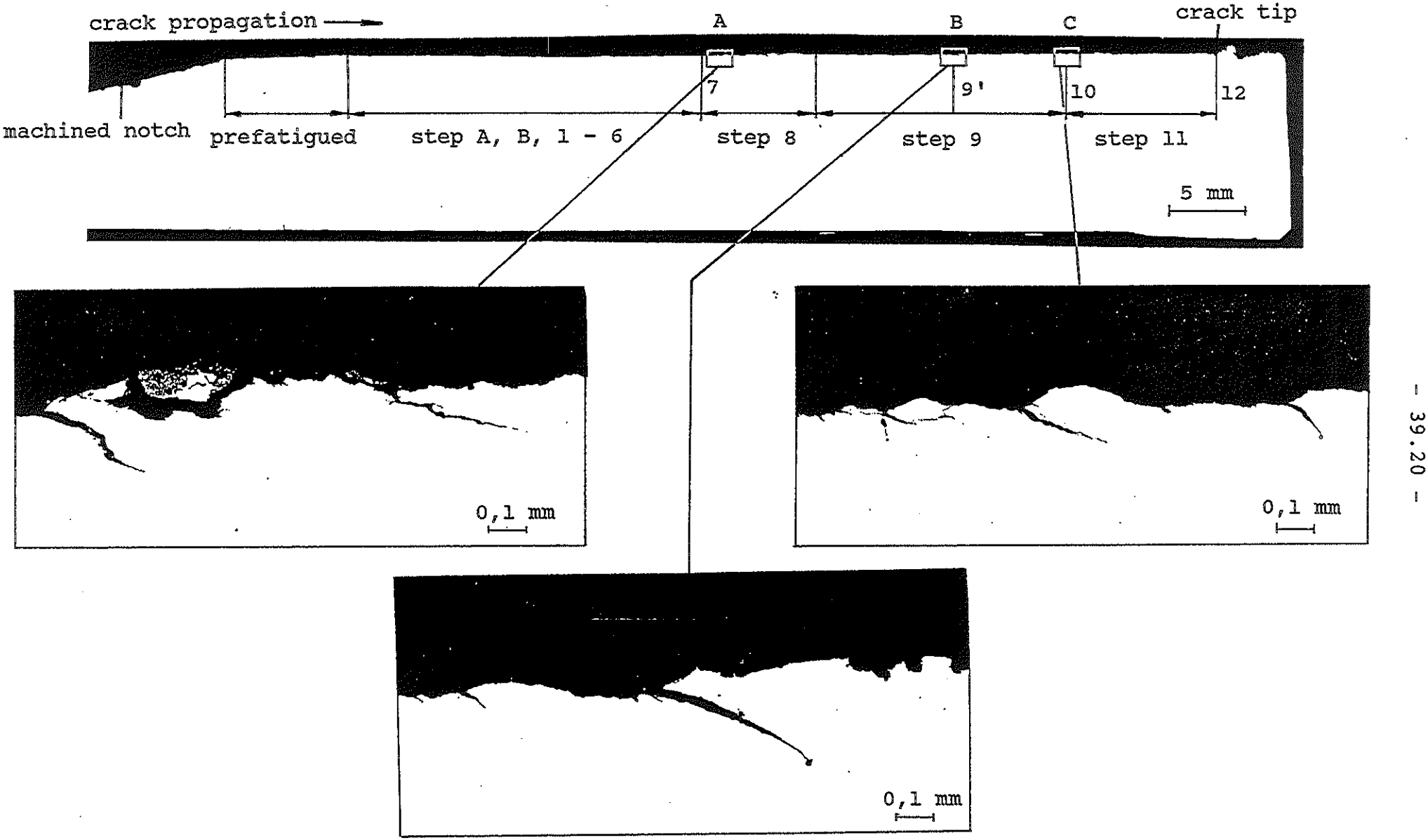

Fig. 6: Crack propagation of longitudinal flaw B, view A of Fig. 5

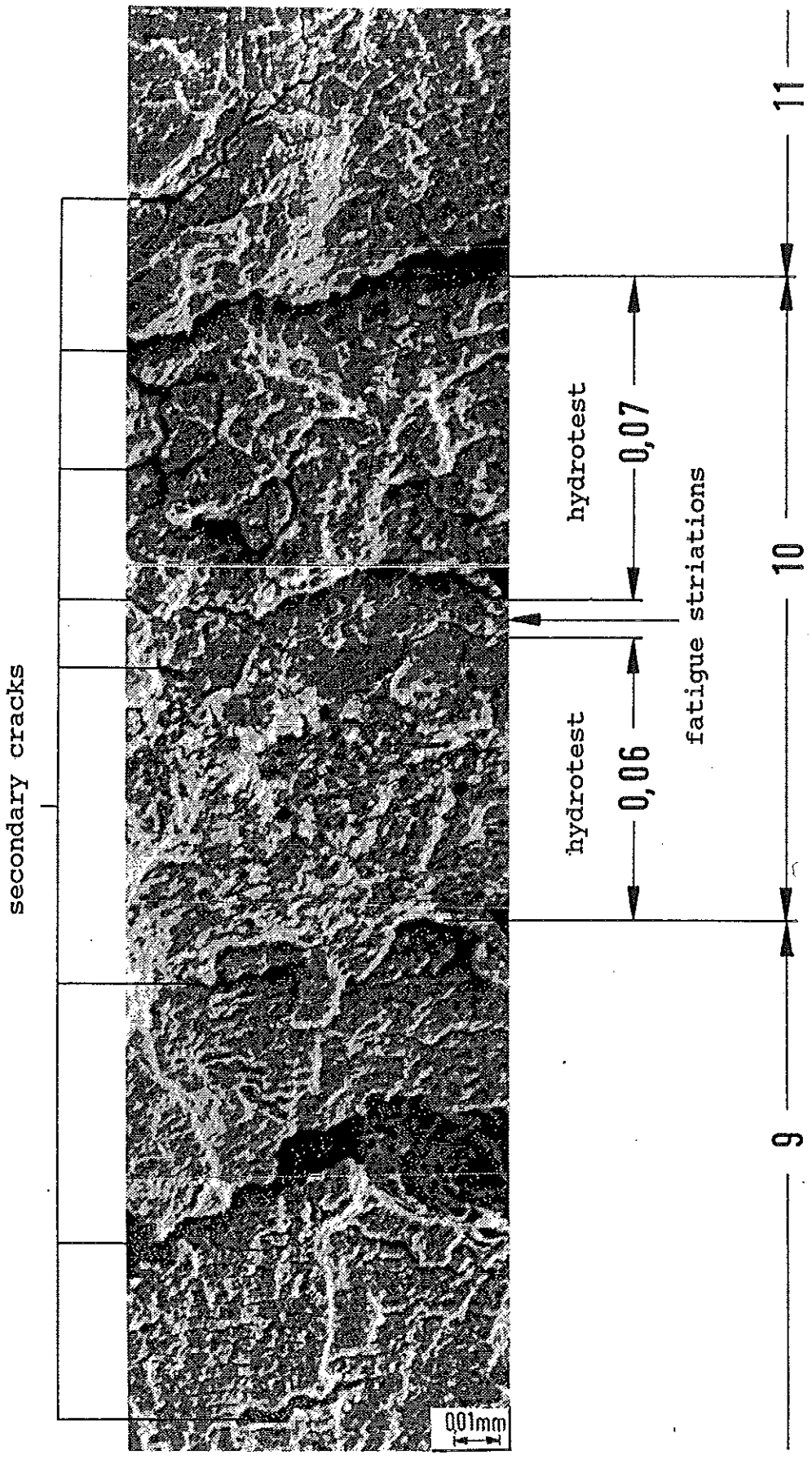

Fig. 7: Section B of Fig. 5, crack growth during cyclic loading and hydrotests

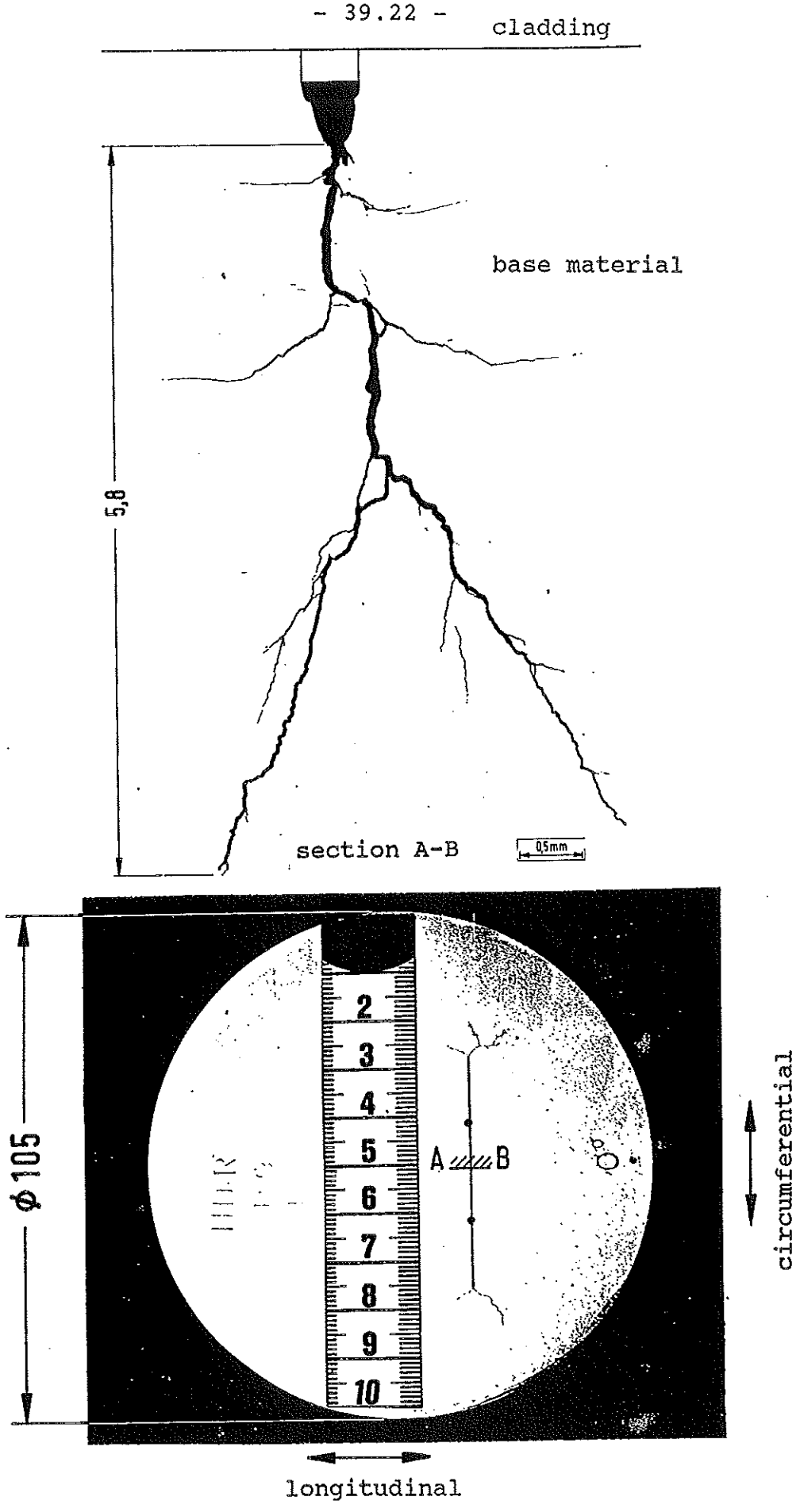

Fig. 8: Trepan B9 of the decommissioned HDR-plant,
inner surface of the cylindrical pressure vessel wall

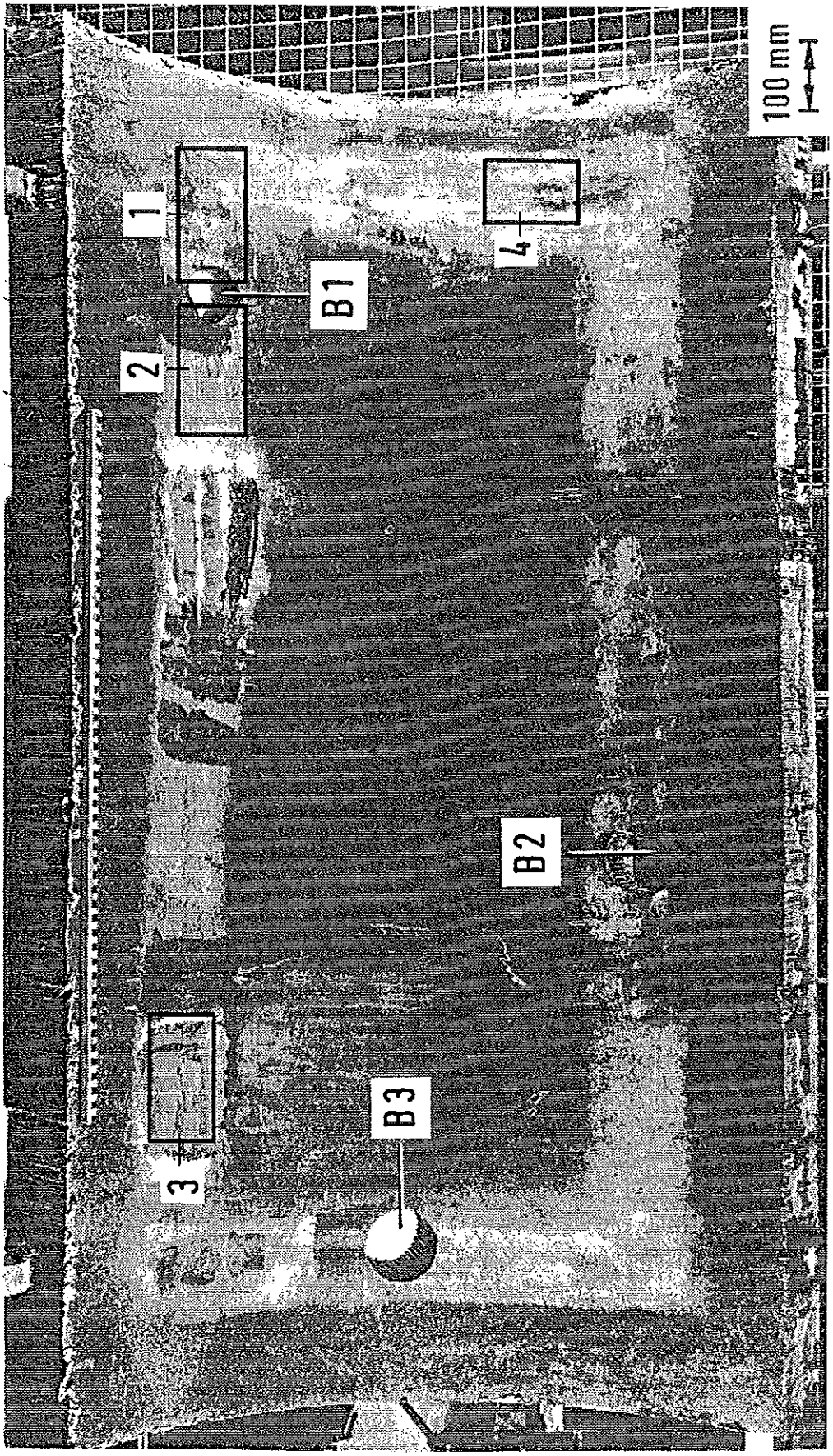

Fig. 9: Inner surface of patch S3, material 20 MnMoNi 5 5,
location of the trepans B1 through B3 and the areas 1 through 4

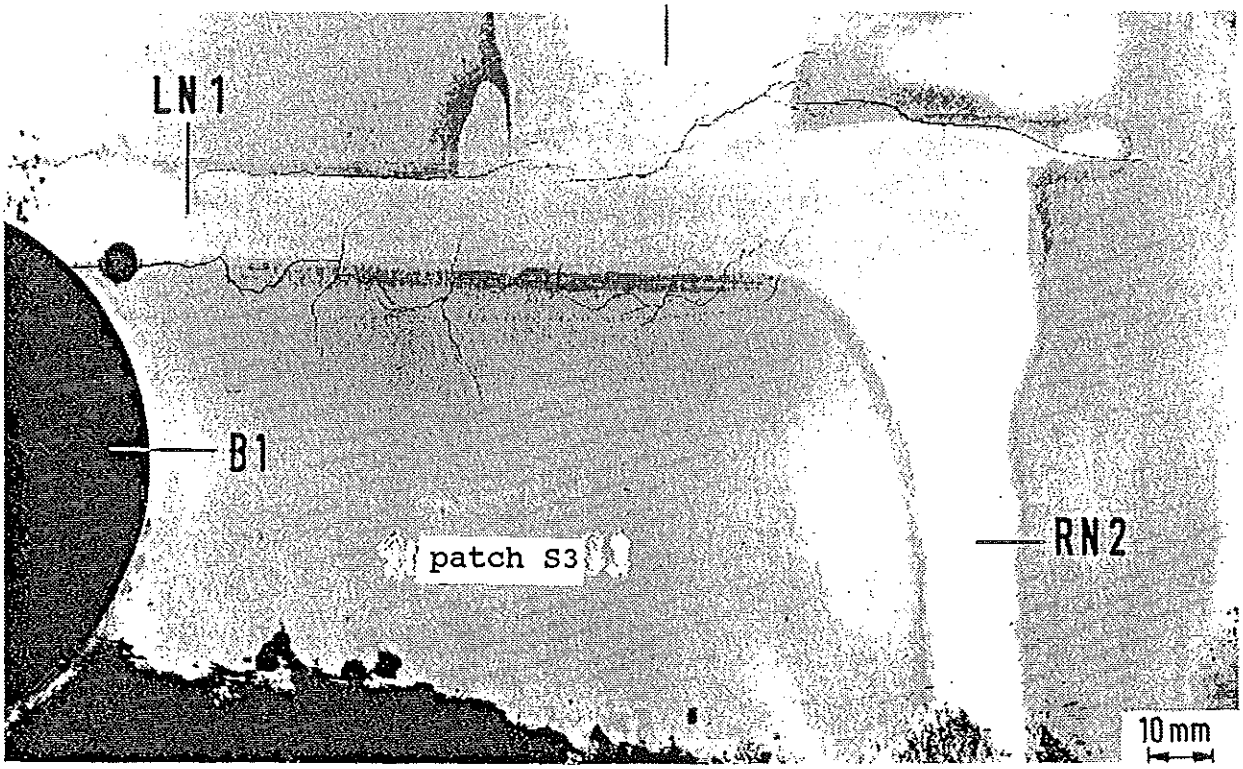

LN 1: longitudinal weld no. 1
RN 2: circumferential weld no. 2

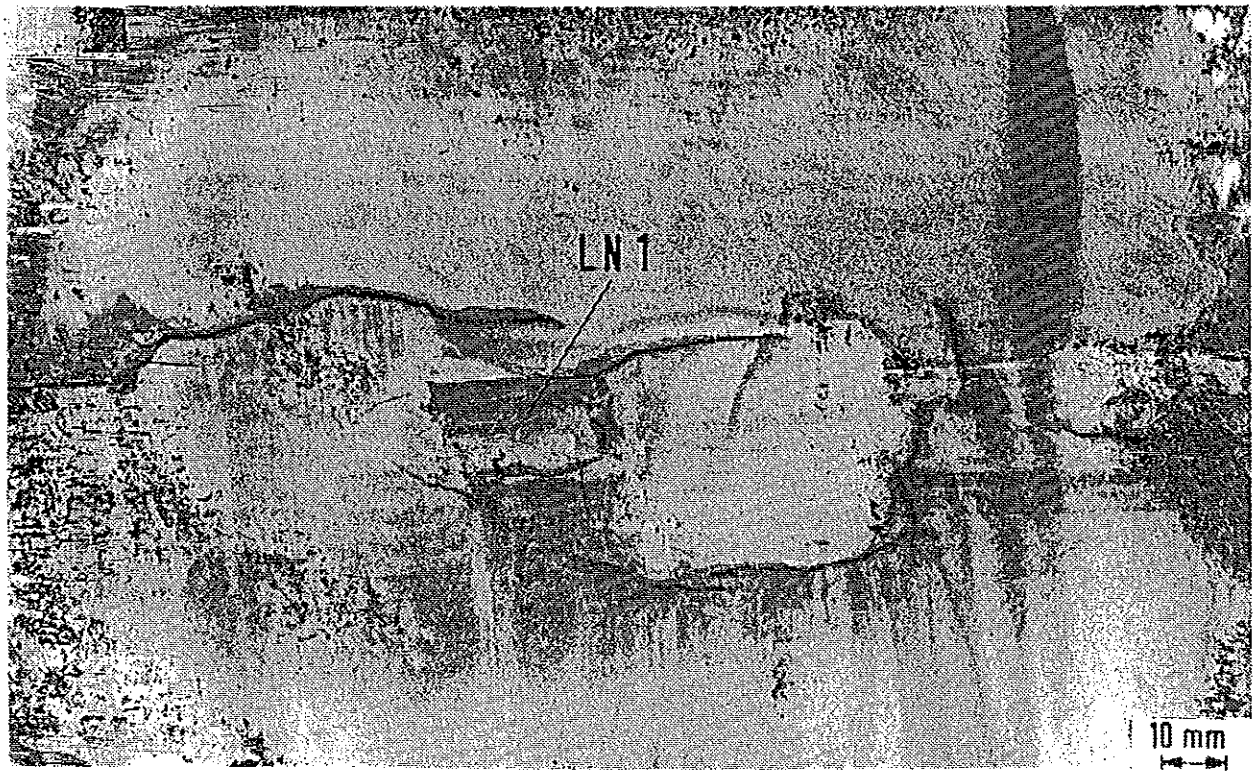

Fig. 10: Fracture appearance in the root of longitudinal weld LN 1,
top: section 1 of Fig. 9
bottom: section 3 of Fig. 9

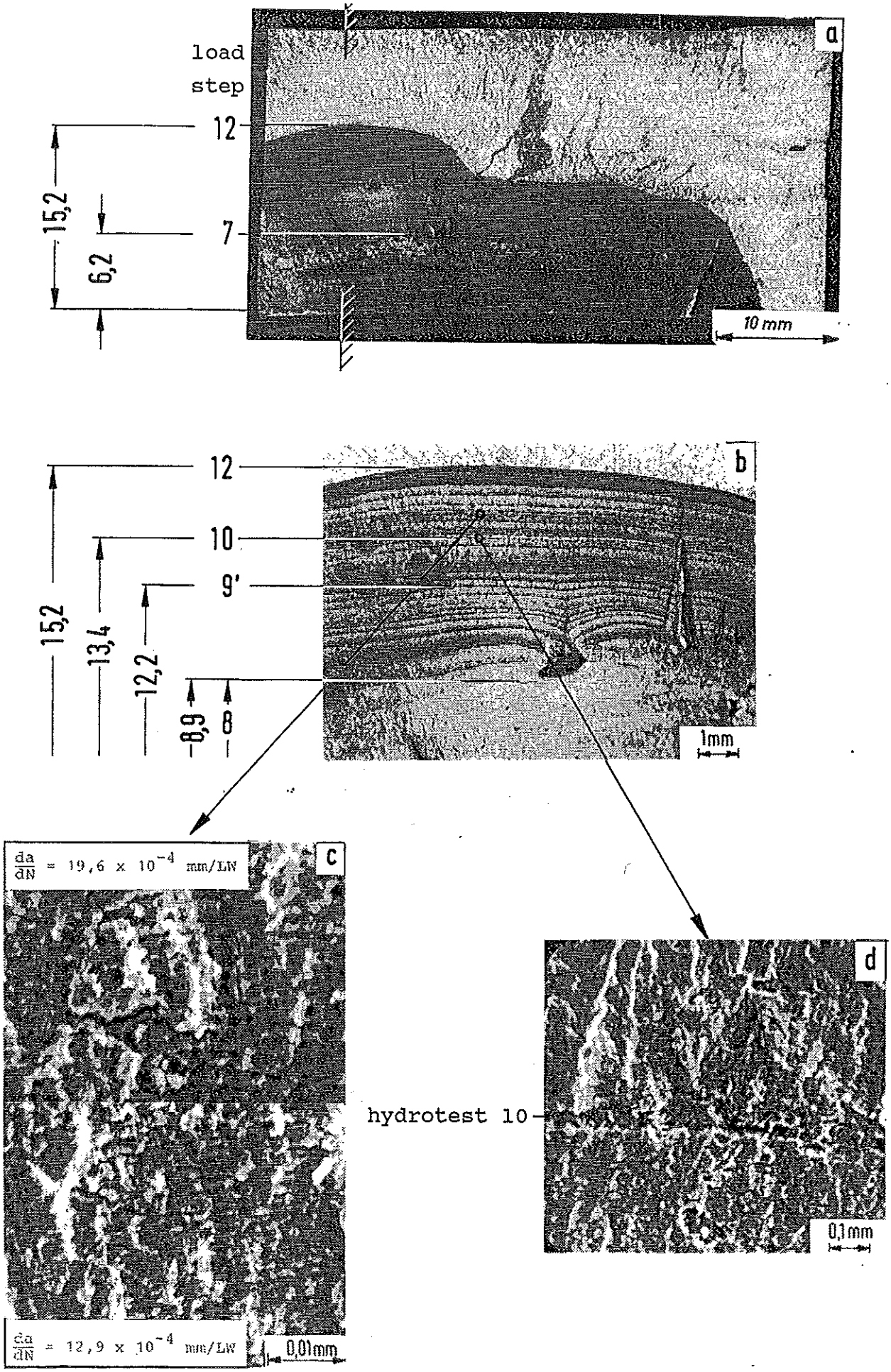

Fig. 11: Longitudinal crack in trepan B2 of Fig. 9

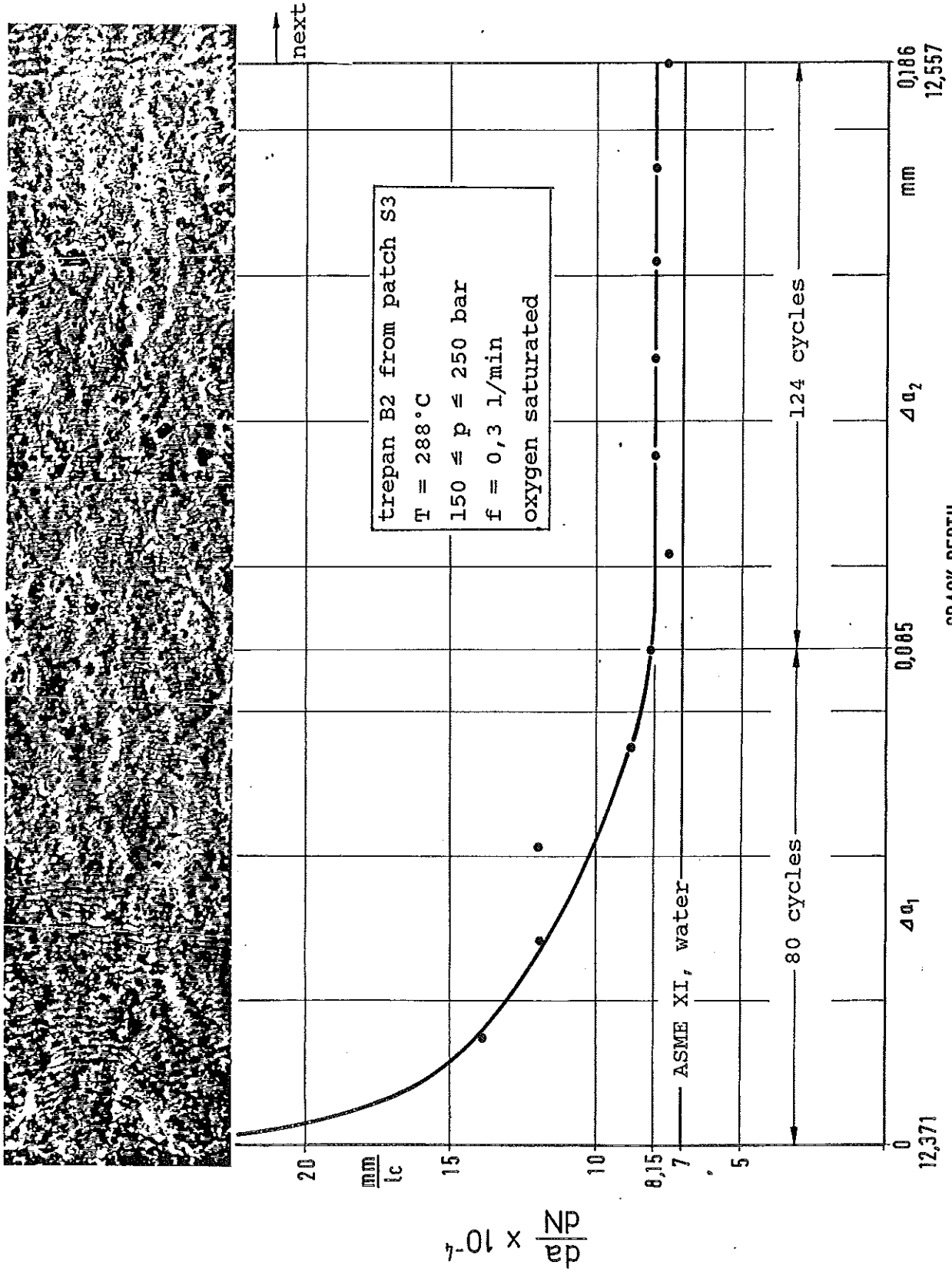

Fig. 12: Cyclic crack growth during one test day after a stop of 18 days, load step 9

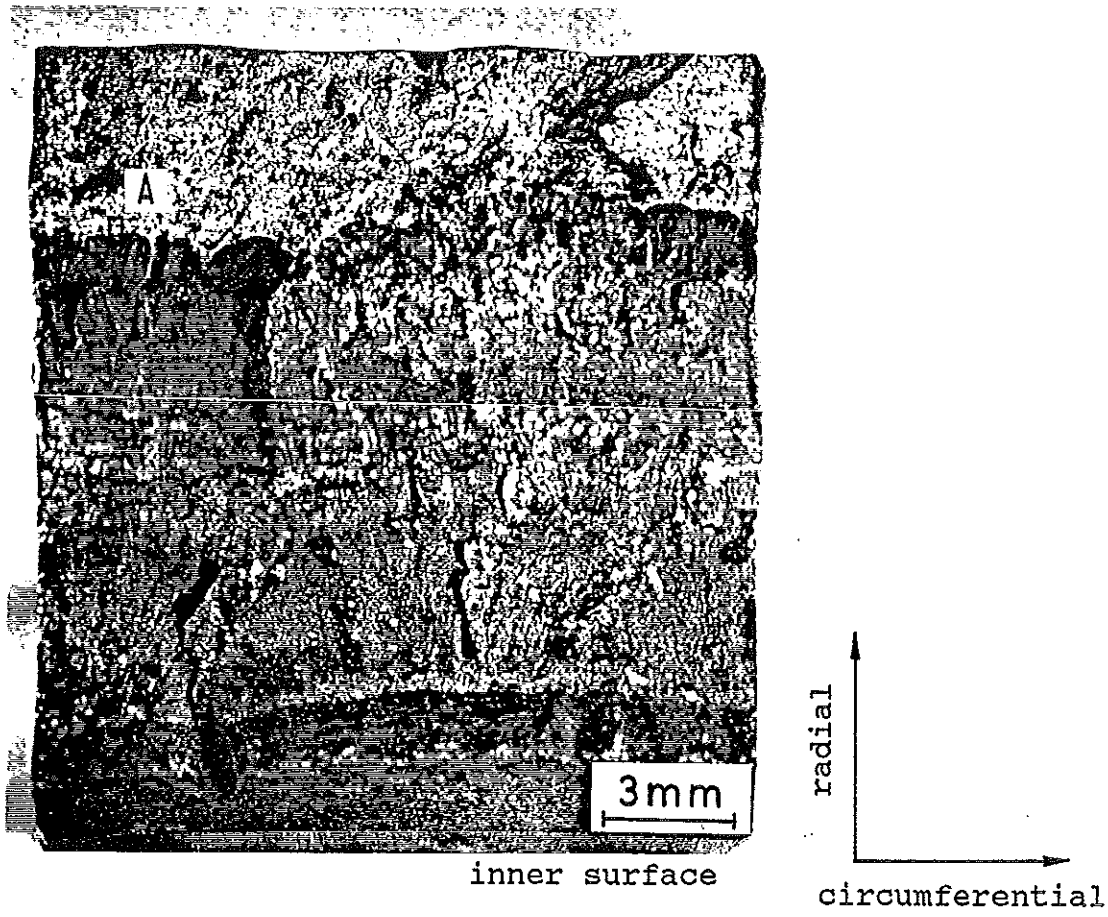

Fig. 13: Circumferential crack from section 4 of Fig. 9

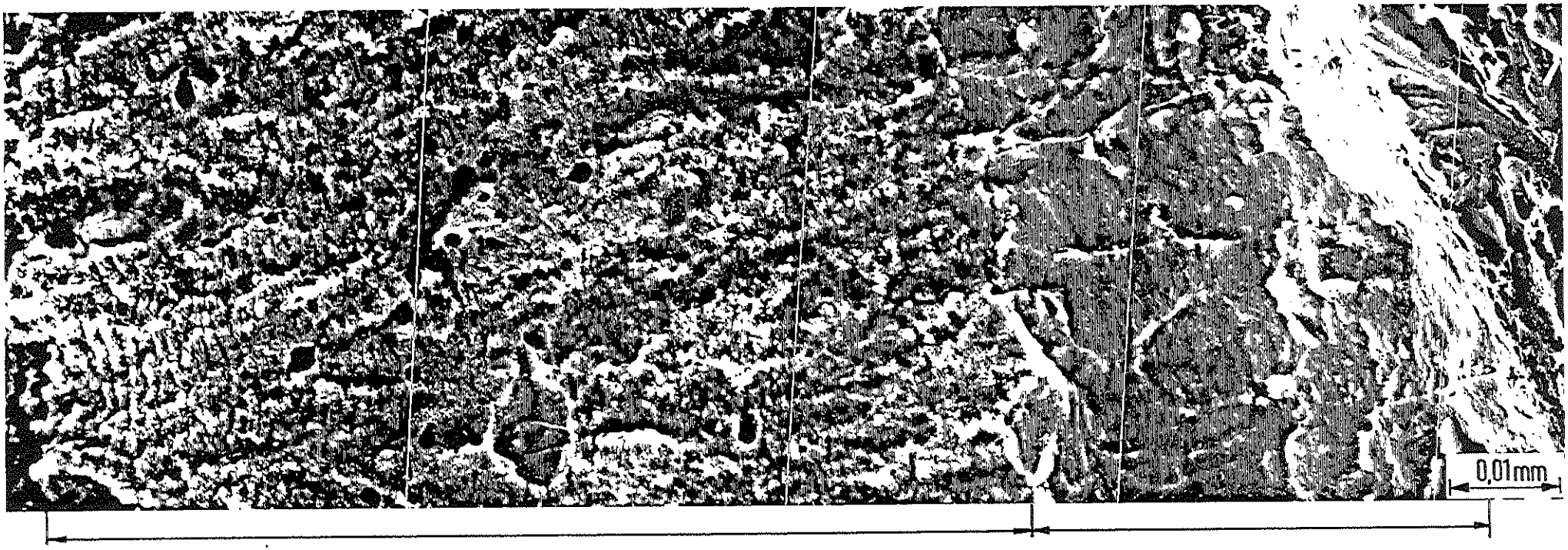

Fig. 14: Crack growth by cyclic loading at 288°C and hydrotest at 60°C, section A of Fig. 13